Spectrally Encoded Coherence Tomography and Reflectometry (SECTR): simultaneous *en face* and cross-sectional imaging at 2 gigapixels-per-second

Mohamed T. El-Haddad, Ivan Bozic, Yuankai K. Tao[*]

Department of Biomedical Engineering, Vanderbilt University, Nashville, TN 37235, USA
[*] Corresponding author: yuankai.tao@vanderbilt.edu

Supplementary Information

Supplementary Note 1: Suppression of end-face reflection back-coupling

As explained in Section 2.3, a major limitation of illumination and collection through the core and inner-clad of double-clad fibers (DCFs), respectively, is the strong fiber end-face reflection that dominates sample backscattering in direct-detection imaging modalities. We mitigate end-face reflections by index-coupling a flat-polished DCF to the flat face of a wedge prism (Fig. 1(c), middle and right). By optimizing the wedge prism thickness and angle, we spatially offset the dominant glass-air interface reflection to minimize coupling into the DCF inner-clad (Fig. 1(c), right). A wedge prism with 3 mm base thickness and 11.2° angle (PS812-B, Thorlabs) was used. The SER signal was measured before and after coupling to the wedge prism, and a factor of >12.5x reduction in the mean background signal was observed (Fig. S1).

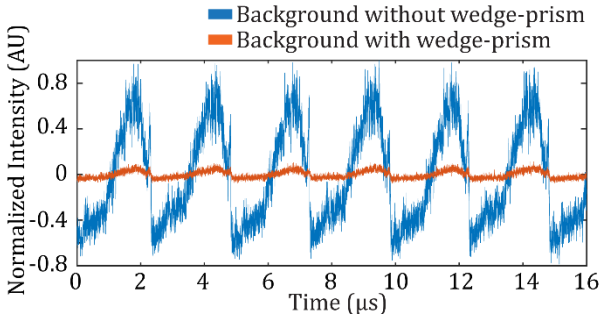

Figure S1 Plot of background signal shows >12.5x reduction in the mean intensity due to back-coupled fiber end-face reflections.

Supplementary Note 2: Multimodality motion-tracking and multi-volumetric mosaicking

Orthogonal priority acquisition planes in OCT (x-z) and SER (x-y) with inherent spatiotemporal co-registration makes SECTR uniquely suited for motion artifact free *in vivo* volumetric imaging. As a proof-of-concept, we demonstrated three-dimensional motion-tracking in post-processing using *in vivo* retinal data (Fig. S2). Inter-frame translational and rotational bulk-motions in the x-y plane were estimated by registering sequential SER frames using discrete Fourier transform [1] and adaptive log-polar transform [2] based rigid-body algorithms. Similarly, translational and rotational motions in the orthogonal x-z plane were estimated from adjacent OCT frames acquired during volumetric imaging. The resulting three-dimensional tracking data showed the fast dynamics of a saccadic eye movement, which was defined here as a step- or impulse-like SER translation with a magnitude >1 standard-deviation. A saccadic movement along the x-axis was observed in both the OCT and SER data (Fig. S2, red arrows). In the same dataset, SER tracking

showed saccadic movement along the y-axis, which was orthogonal to the OCT priority acquisition direction. As expected, the corresponding OCT motion-tracking data showed no detectable motion (Fig. S2, green arrow). This data demonstrated the advantage of multimodality imaging with micron spatial and millisecond temporal resolution for identifying three-dimensional motion artefacts that may otherwise be undetectable when imaging with only OCT or SER (Visualization S1).

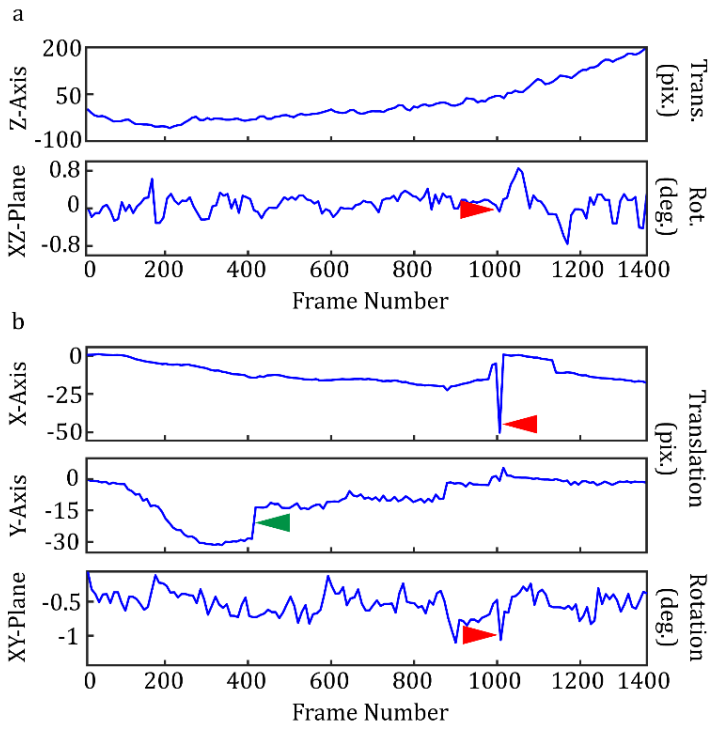

Figure S2 Motion-tracking results from raw (a) OCT and (b) SER frames. A saccade in the x-axis (red arrows) was observed as OCT rotational and SER translational/rotational motions. A saccade in the y-axis (green arrow) was orthogonal to the OCT fast-axis and only observed on SER (Visualization S1).

An additional advantage of this acquisition scheme is that it facilitates mosaicking of ultrawide-field volumetric datasets, as explained in Section 2.7. Using the *en face* SER motion information, all frames in each volume were registered to the first frame of the central volume; a volume that shows the optic nerve head (ONH) in the center of the FOV. Registration information from the SER data was also used to compensate for inter-B-scan bulk-motion. Similarly, OCT motion information was used to correct for axial bulk-motion in each volume. Finally, OCT B-scans were processed to flatten the retinal layers to eliminate inter-volume tilt and curvature variations, and enable volumetric mosaicking.

Flattening of the retinal layers was performed by segmenting the retinal pigment epithelium (RPE) based on pixel intensity and connectivity [3]. First, each OCT B-scan was low-pass filtered, and a vertical gradient was calculated to emphasize layer boundaries (Fig. S3(b)). The location and extent of the highly reflective Nerve Fiber Layer (NFL) were estimated by finding the first two intensity peaks along each A-scan in the gradient image. The NFL was then masked down to an empirically determined depth to remove reflections from the upper retinal layers. This guaranteed that the remaining bright reflections were confined to the RPE, which was then segmented by performing another peak search along each A-scan in the masked image (Fig. S3(c)). At the ONH, the RPE was approximated as a second-degree polynomial that connected the RPE layers on both sides of the ONH boundaries, which were estimated as points of large variation (>15 standard deviations) in the first derivative of the segmented RPE (Fig. S3(c)). Finally, the segmented RPE was flattened by applying vertical pixel shifts along each A-scan (Fig. S3(d)). While the segmentation output in the background regions was arbitrarily determined by the residual background noise (Fig. S3(c), white arrowheads), it did not affect the final flattening result.

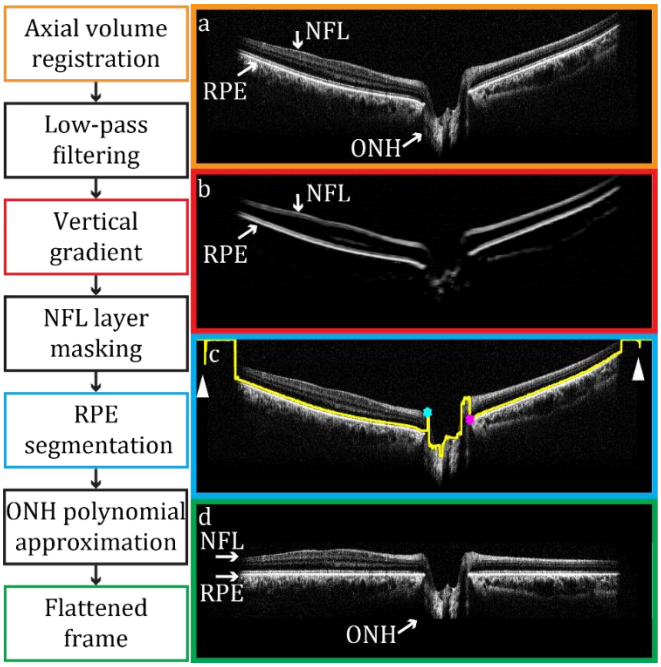

Figure S3 OCT B-scan flattening algorithm. (a) Representative OCT cross-section. (b) Vertical gradient of the OCT frame. (c) Segmented RPE layer (yellow line) and ONH boundaries (cyan and magenta asterisks). White arrowheads show segmentation output in background regions. (d) OCT frame after RPE flattening. NFL, nerve fiber layer; ONH, optic nerve head, RPE, retinal pigment epithelium.

Supplementary Note 3: *In vivo* human ophthalmic imaging of the anterior chamber

In vivo SECTR imaging was demonstrated in a healthy volunteer under an IRB-approved protocol. The power incident at the pupil was 1.3 mW for OCT and 2.65 mW for SER. OCT volumes were sampled with 2560 x 2000 x 1400 pix. (spectral x lateral x lateral) in 7 s, and corresponding SER images were sampled with 2560 x 2000 pix. (spectral x lateral) acquired at 200 fps (Fig. S4). High frame-rate SER images provided *en face* views of anatomic structures for aiming and fixation and showed sample motion dynamics from pupil dilation (iris). The cornea, iris, and anterior lens capsule were clearly resolved on anterior segment OCT. Comparison of respective anatomic landmarks between *en face* OCT volume projection and SER images shows spatiotemporal co-registration of overlapping field-of-views (FOVs) (Visualization S2).

Supplementary Note 4: OCT imaging range

High-speed digitization of the laser sweeps at 1.2 GHz enabled long axial range OCT imaging of semi-transparent structures over more than 7 mm in depth. As a demonstration of the utility of long-range imaging, anterior segment imaging shows OCT cross-sections of the entire corneal curvature, structures in the pupil, and the anterior lens capsule (Fig. S4(c)) without the need for complex-conjugate ambiguity resolved imaging or complex detection methods [4–6]. Similarly, the long -6 dB fall-off range allowed us to image the weakly scattering layers of the cornea with incident light levels below the ANSI MPE.

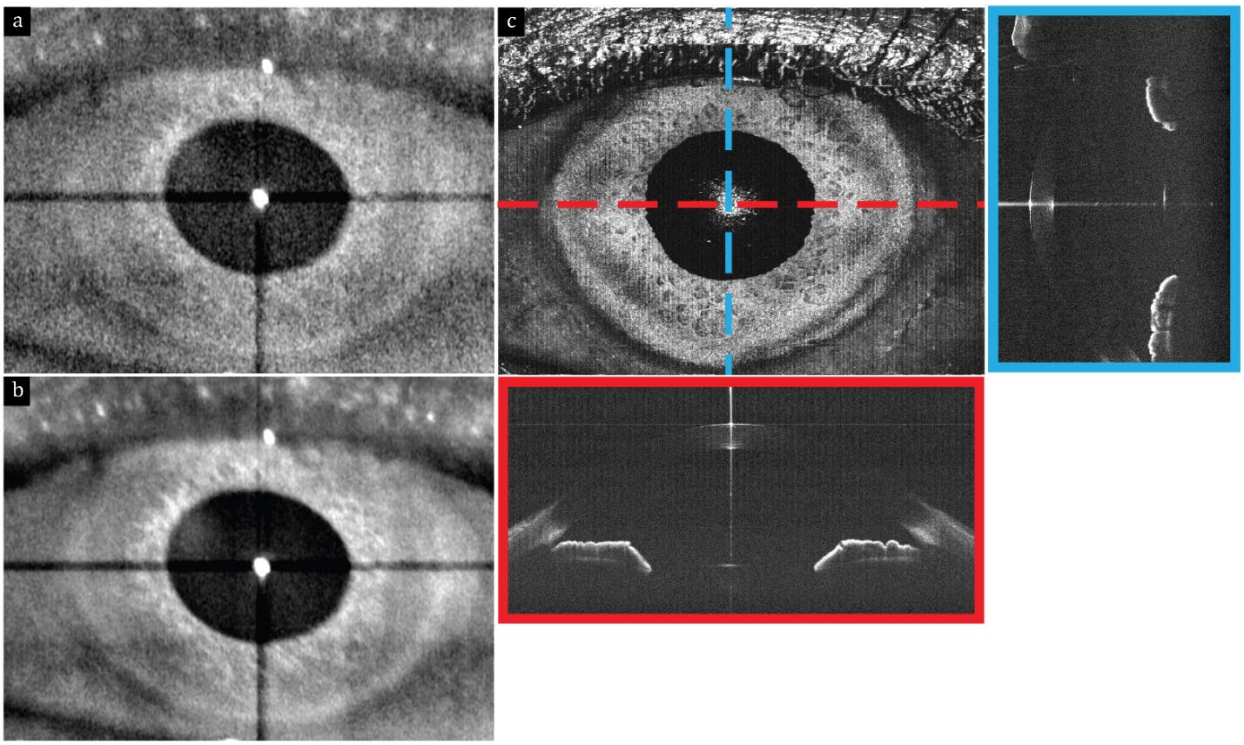

Figure S4 *In vivo* SECTR imaging of the anterior chamber in a healthy volunteer (Visualization S1). (a) Raw and (b) 5-frame average of 2560 x 2000 pix. (spectral x lateral) SER images acquired at 200 fps. (c) *En face* OCT volume projection with representative fast- and slow-axis cross-sections (red and blue, respectively) showing the entire corneal curvature, structures in the pupil, and the anterior lens capsule. OCT volume was sampled with 2560 x 2000 x 1400 pix. (spectral x lateral x lateral) in 7 s.

Supplementary Note 5: Optical bandwidth losses

The Axsun 1060 nm swept-source used in our SECTR system had a 105 nm optical bandwidth, which corresponds to a theoretical OCT axial PSF FWHM of 4.7 µm in air and 7.1 µm after Gaussian spectral reshaping for optimal side-lobe suppression. Our experimentally measured axial PSF FWHM was 1.6x larger than theoretical predictions because of spectral subsampling. The duty cycle of the laser was 63%, which resulted in the loss of 21% of the full sweep-range after optical buffering because of spectral overlap between the original and buffered sweeps. In addition, 3000 samples were required to sample a full 400 kHz sweep at 1.2 GHz k-clock rate. However, our high-speed digitizer required 1) the number of acquired samples to be an integer multiple of 128, and 2) an overhead of 256 samples per acquisition to re-arm the trigger. Thus, each acquisition was limited to a maximum of 2560 samples to avoid missing any triggers due to laser jitter. These sampling constraints limited the net acquisition throughput to 2 gigapixels-per-second, and resulted in an additional 15% loss in total recorded spectral bandwidth for a final acquired sweep range of 70 nm. At this bandwidth, the theoretical OCT axial PSF had a FWHM of 7.1 µm (10.7 µm after spectral reshaping), which was well-matched to our experimental results (Fig. 4). In SER, reduced spectral bandwidth resulted in FOV clipping along the spectrally-encoded dimension (Fig. 5 (a), (b)). These losses in resolution and FOV may be avoided by implementing SECTR using a swept-source with less than 50% duty cycle. However, the optimal clock speed would need to be increased accordingly to ensure the full spectral bandwidth is critically sampled for SER.

Supplementary Note 6: Power losses and sensitivity

The theoretical shot-noise limited SNR of our OCT was 101.8 dB assuming no insertion-losses between the sample and detector [7,8]. The difference between the theoretical and measured 96 dB SNR was attributable to fiber-optic coupling losses at physical contact connector faces. Fusion-splicing all fiber-optic connections in future implementations of SECTR should reduce losses and enable near shot-noise limited SNR performance.

Supplementary Note 7: Functional imaging

While both SECTR modalities are only sensitive to scattering contrast, functional imaging is also possible by taking advantage of speckle or phase contrast to vascular perfusion. Established methods for Doppler OCT and OCT angiography may be directly applied to SECTR imaging by modifying galvanometer scan waveforms and implementing corresponding post-processing algorithms [9–12]. We believe the ability of SECTR to track three-dimensional motion may provide significant improvements over existing bulk-motion compensation algorithms conventionally used for functional OCT.

References

[1] M. Guizar-Sicairos, S.T. Thurman, and J.R. Fienup, Opt. Lett., 33, 156–158 (2008).
[2] R. Matungka, Y.F. Zheng, and R.L. Ewing, IEEE Trans. Image Process., 18, 2340–2354 (2009).
[3] Q. Yang, C.A. Reisman, Z. Wang, Y. Fukuma, M. Hangai, N. Yoshimura, A. Tomidokoro, M. Araie, A.S. Raza, D.C. Hood, and K. Chan, Opt. Express, 18, 21293–21307 (2010).
[4] A.-H. Dhalla and J.A. Izatt, Biomed. Opt. Express, 2, 1218–1232 (2011).
[5] M.V. Sarunic, M.A. Choma, C. Yang, and J.A. Izatt, Opt. Express, 13, 957–967 (2005).
[6] Y.K. Tao, M. Zhao, and J.A. Izatt, Opt. Lett., 32, 2918–2920 (2007).
[7] J.F. de Boer, B. Cense, B.H. Park, M.C. Pierce, G.J. Tearney, and B.E. Bouma, Opt. Lett., 28, 2067–2069 (2003).
[8] T. Klein, W. Wieser, L. Reznicek, A. Neubauer, A. Kampik, and R. Huber, Biomed. Opt. Express, 4, 1890–1908 (2013).
[9] Z. Chen, M. Liu, M. Minneman, L. Ginner, E. Hoover, H. Sattmann, M. Bonesi, W. Drexler, and R.A. Leitgeb, Biomed. Opt. Express, 7, 3032–3048 (2016).
[10] I. Gorczynska, J.V. Migacz, R.J. Zawadzki, A.G. Capps, and J.S. Werner, Biomed. Opt. Express, 7, 911–942 (2016).
[11] Y. Jia, J.C. Morrison, J. Tokayer, O. Tan, L. Lombardi, B. Baumann, C.D. Lu, W. Choi, J.G. Fujimoto, and D. Huang, Biomed. Opt. Express, 3, 3127–3137 (2012).
[12] B. Braaf, K.V. Vienola, C.K. Sheehy, Q. Yang, K.A. Vermeer, P. Tiruveedhula, D.W. Arathorn, A. Roorda, and J.F. de Boer, Biomed. Opt. Express, 4, 51–65 (2013).